Journal of Luminescence 204 (2018) 633–641

Contents lists available at ScienceDirect

Journal of Luminescence

journal homepage: www.elsevier.com/locate/jlumin

Synthesis and study of $(Ca/Ba)_{0.45}Eu_{0.05}Zr_2(PO_4)_3$ nanophosphors and $(Ca/Ba)_{0.45}Eu_{0.05}Zr_2(PO_4)_3@SiO_2$ nanostructures with blue-green emission

J. Isasi[a,*], L. Alcaraz[a], P. Arévalo[a], C. Gumiel[b], M. Peiteado[c]

[a] Departamento de Química Inorgánica I, Facultad de Ciencias Químicas, Universidad Complutense de Madrid, Ciudad Universitaria s/n, 28040 Madrid, Spain
[b] POEMMA-CEMDATIC, ETSI Telecomunicación (UPM), Avda. Complutense 30, 28040 Madrid, Spain
[c] Departamento de Electrocerámica, Instituto de Cerámica y Vidrio (CSIC), Kelsen, 5, 28049 Madrid, Spain

ARTICLE INFO

Keywords:
Sol-gel processes
Nanostructured materials
Optical materials
Optical properties

ABSTRACT

$M_{0.45}Eu_{0.05}Zr_2(PO_4)_3$ nanophosphors with M = Ca or Ba were prepared by a two-steps process including the use of a sol-gel process under basic conditions followed by treatment in a N_2/H_2 reducing atmosphere. $Ca_{0.45}Eu_{0.05}Zr_2(PO_4)_3$ sample were also obtained by treatment in a N_2 flow. The corresponding $M_{0.45}Eu_{0.05}Zr_2(PO_4)_3$ @SiO_2 nanocomposites were synthetized by treatment with tetraortoethylsilicate (TEOS). The effects of calcium by barium substitution on the samples were analyzed by X-ray diffraction (XRD), Fourier transform infrared (FTIR) and transmission electron microscopy (TEM). TEM-energy dispersive spectroscopy (EDS) analyses were carried

out by using an OXFORD INCA instrument. In addition, magnetic behavior, photoluminescence emission spectra and Commission International de I'Eclairage (CIE) of these phosphors were analyzed by magnetic susceptibility measurements and photoluminescence (PL) spectroscopy, respectively. XRD patterns of synthesized samples can be indexed according to a rhombohedral symmetry of space group R-3 with $Z = 6$, compatible with a NASICON-type structure. FTIR spectra of the covered samples show some bands attributed to Si-O bending vibration and additional characteristics of vibration modes of PO_4^{3-} units. Nanoparticles covered by a silica shell were found in TEM micrographs of $M_{0.45}Eu_{0.05}Zr_2(PO_4)_3$ @SiO_2 whose thickness depends on its reaction time with TEOS. Magnetic measurements confirm the state oxidation of europium ions in the all luminescent cores. PL measurements show a variation of the emission intensity related to both the replacement of calcium by barium and the different thicknesses of the silica shell.

1. Introduction

The study of phosphors and, particularly, the solid-state lighting (SSL) based on rare earth-doped orthophosphate has become a subject of great interest because of their potential applications to a wide variety of optoelectronic devices such as photovoltaic applications and white light generation via Hg-free lamps [1–4]. At present, the light provided by these materials has become a promising alternative to conventional incandescent and fluorescent lamps for illumination [5]. The optical properties of these materials are usually originated from complicated interactions between host lattice, activators and defects, being of essential importance the contribution of the host network on the optical properties [5–7]. These luminescent materials offer a high light yield with low energy consumption [8–13].

Some studies have determined that Eu^{2+}-activated orthophosphates are useful for visible and UV radiation sources as well as for white LEDs devices [6,7]. These studies have also found that under UV excitation the emission spectrum of Eu^{2+} cations is centered in the blue range of the visible spectrum. This emission is generally attributed to $4f^65d^1$–$4f^7$ electronic transitions [6,7]. However, various factors such as site symmetry, the nature of the coordinating anions, the coordination number and the nature of the next nearest cation neighbours have an influence on the position of the 4f-5d states. For these reasons, a further investigation on the f-d transitions of the rare-earth ions in the different host lattices was necessary.

The NASICON-type structure of orthophosphates $M_{0.45}Eu_{0.05}Zr_2(PO_4)_3$ with M = Ca^{2+}, Sr^{2+} y Ba^{2+} shows suitable advantages for the activated luminescent material containing Eu^{2+}. These advantages include high thermal stability, long distances between M^{2+} ions and adjustable chemical composition. NASICON-type phosphate materials have been the focus of attention due to their excellent electrochemical performance and versatile structure, so they have been

* Corresponding author.
E-mail address: isasi@ucm.es (J. Isasi).

https://doi.org/10.1016/j.jlumin.2018.08.082
Received 4 June 2018; Received in revised form 15 August 2018; Accepted 29 August 2018
Available online 30 August 2018
0022-2313/

widely investigated as ionic conductors [14,15] or low thermal expansion ceramics [16,17], however few reports are focused on their optical properties [6,18–20]. In relation to its optical properties, other authors have described that these depend not only on the specific host lattice and on the environment of the activator ions, but also on the size, shape and organization of the constituent phosphor particles. [7,21,22], so it has been proved that the variation of the luminescent signal is dependent on its morphology, since the particle size affects the intensity of luminescence, being high in bigger particles or, referring to its structure, micro-belts nanophosphors have a higher intensity than nanofiber phosphors [5–7].

With the aim of obtaining lanthanide-doped $M_{0.5-}xEu_xZr_2(PO_4)_3$ nanophosphors with high quantum yields for use in certain applications, different synthesis methods including solid state reactions [22,23], co-precipitation methods [24,25] or sol-gel process [6,7] have been developed over the years. Unfortunately, in the first two cases the requirement of high temperature treatments leads to an increase of the particle size which also results in the obtaining of agglomerated powders. Contrary, the development of new sol-gel processes currently enables the synthesis of non-agglomerated nanoparticles with more uniform morphologies using relatively low (to mild) temperatures. Such processes have been already been tested by the authors of this present manuscript for the synthesis of compounds with other stoichiometry and doped with different rare earth ions [26–29].

It should be noted that, in some circumstances during the synthesis stage, the luminescent nanoparticles, can develop defects on their surface, which can affect their luminescent properties (via non radiant energy loss), reducing the quantum efficiency of the synthesized nanophosphors. Occasionally, core-shell structures have been used to correct the problem caused by defects present on the surface of luminescent nanoparticles [30,31]. Silica has been widely used as an efficient coating due to its high chemical stability, optical transparency, easily controllable shell thickness, low cytotoxicity and biocompatibility [31,32]. Moreover, silica covering will provide chemical stability to the phosphor nucleus, protecting it from oxidation and thus reducing the mentioned loss of emission [33]. In this frame, the aim of the present work is to describe the synthesis of $M_{0.45}Eu_{0.05}Zr_2(PO_4)_3$ @SiO_2 samples, with M = Ca or Ba, by a sol-gel process under basic conditions and through the subsequent use of the Stöber method. In a comparative way, the effects of the partial calcium substitution by barium ions and the different synthesis conditions used to obtain the two calcium samples on the crystal structure, powder morphology, optical and magnetic properties have been assessed.

2. Material and methods

$M_{0.45}Eu_{0.05}Zr_2(PO_4)_3$ with M = Ca or Ba samples were synthesized by sol-gel process. In addition, $M_{0.45}Eu_{0.05}Zr_2(PO_4)_3$ @SiO_2 composites were prepared by Stöber method in order to obtain an homogeneous shell around the luminescent nanoparticles.

2.1. Synthesis of luminescent cores

$M_{0.45}Eu_{0.05}Zr_2(PO_4)_3$ samples with M = Ca or Ba were synthesized by a two-step process including the use of a sol-gel process under basic conditions, followed by a treatment in a N_2/H_2 reducing atmosphere to stabilize the 2 + oxidation state of europium. In addition, for comparison purposes, $Ca_{0.45}Eu_{0.05}Zr_2(PO_4)_3$ sample was prepared as previously describe, but under a N_2 flow. In this sample, it is expected that europium presents a mixed oxidation state (2 + and 3 +).

For these preparations, calcium nitrate ($Ca(NO_3)_2{\cdot}4H_2O$, (99%, Sigma Aldrich)), barium nitrate ($Ba(NO_3)_2$ (99,5%, Strem Chemical)), europium nitrate ($Eu(NO_3)_2{\cdot}6H_2O$, (99,9%, Strem Chemical)), zirconium acetylacetonate ($Zr(CH_2COCH_2COCH_3)_4$, (for synthesis, Merck)) and ammonium phosphate ($NH_4H_2PO_4$, ($\geq$ 98%, Sigma Aldrich)) were employed as starting precursors. In addition, citric acid ($C_6H_8O_7$ (CA) (99.5% Panreac)) and ethylene glycol ($C_2H_6O_2$ (EG) (99%, Sigma Aldrich)) were used as chelating and polymeric agents, respectively. Stoichiometric amounts of each reagent were dissolved in distilled water. pH value of the resulting solutions was initially adjusted to 2 by the addition of citric acid solution, prepared according to a molar ratio $\Sigma[CA]/\Sigma[\text{metal atoms}] = 2$ and then, the pH value was adjusted to 10 by NH_3 addition (25% Sigma Aldrich). Ethylene glycol with a molar ratio $\Sigma[AC]/\Sigma[EG] = 1$ was slowly added on the solutions to generate weak interactions between particles during crystallization to produce gels. These gels were aged for 4 days and dried at 423 K for 24 h to obtain the corresponding precursor powders. These precursors were treated at 898 K for 24 h to completely remove organic matter.

In a second step, to achieve the reduction of Eu^{3+} to Eu^{2+}, the precursor powder of $Ba_{0.45}Eu_{0.05}Zr_2(PO_4)_3$ composition was treated at 1023 K during 12 h under a N_2/H_2 (90:10) reducing atmosphere. $Ca_{0.45}Eu_{0.05}Zr_2(PO_4)_3$ composition samples were prepared in two different ways: 1) the sample was treated as described to the barium sample; and 2) the sample was treated at both same temperature and time, but under N2 atmosphere. In all cases, black color powders were obtained. The synthesized samples are namely as $Ca_{0.45}Eu_{0.05}Zr_2(PO_4)_3$_1 (treated in N_2 atmosphere), $Ca_{0.45}Eu_{0.05}Zr_2(PO_4)_3$_2 and $Ba_{0.45}Eu_{0.05}Zr_2(PO_4)_3$ (both treated in N_2/H_2 atmosphere).

2.2. Synthesis of luminescent composites

The synthesized $M_{0.45}Eu_{0.05}Zr_2(PO_4)_3$ powders were covered with silica (SiO_2) by the Stöber method [34]. 0.025 g of $M_{0.45}Eu_{0.05}Zr_2(PO_4)_3$ powders were dispersed in 50 mL of distilled water, 150 mL of ethanol and 5 mL of ammonia (32%) assisted by a sonicator during 5 min. The addition was performed at a constant speed to obtain a narrow distribution of the particle size. Then, 1 mL of TEOS (synthesis, Merck) was added slowly under magnetic stirring and the reaction was carried out during 3 h in order to analyze the effects of the TEOS reaction time in the microstructure and final properties. The resulting white powders were collected by centrifugation and, then, washed twice with a deionized water/ethanol solution. The synthesized samples are namely as $Ca_{0.45}Eu_{0.05}Zr_2(PO_4)_3$_1@$SiO_2$, $Ca_{0.45}Eu_{0.05}Zr_2(PO_4)_3$_2@$SiO_2$, and $Ba_{0.45}Eu_{0.05}Zr_2(PO_4)_3$@$SiO_2$. In the absence of shell in the sample the $Ba_{0.45}Eu_{0.05}Zr_2(PO_4)_3$ @SiO_2, subsequently, another equivalent sample was prepared by increasing the reaction time of the luminescent barium core with TEOS to 9 h. The synthesized sample is named as the $Ba_{0.45}Eu_{0.05}Zr_2(PO_4)_3$ @SiO_2_9.

2.3. Characterization

The structural characterization of the synthetized samples was carried out by X-ray diffraction (XRD) employing an X´Pert-MPD Phylips difractometer with Cu Kα radiation. Step scan of 0.04° (2θ) in the range 10–70° with a counting time of 1 s for each step were employed for data collection. Powder diffraction data were refined by the Rietveld method using the FullProf software [35] and a Thompson-–Cox–Hastings function to describe the peak shape. The possible association of nanophosphors with silica was evaluated from Fourier transform infrared (FTIR) spectra recorded on an IR-Prestige-21 Fourier Transform spectrometer, with a frequency range resolution of 4 cm^{-1}. All FTIR spectra were measured on the 4000–400 cm^{-1} region for samples dispersed in KBr pellets. Transmission electron microscopy (TEM) images were obtained on a JEOL 2100 F transmission electron microscope, operating at 200 kV and equipped with a field emission electron gun providing a point resolution of 0.19 nm. Samples were prepared by placing a drop of a dilute n-butanol dispersion of nanoparticles onto a 300 mesh carbon coated copper grid. The temperature dependence of the magnetic susceptibility under an applied magnetic field of 1 kOe was measured in the (2 − 300) K range using a Quantum Design XLSQUID magnetometer. Optical properties of the samples were

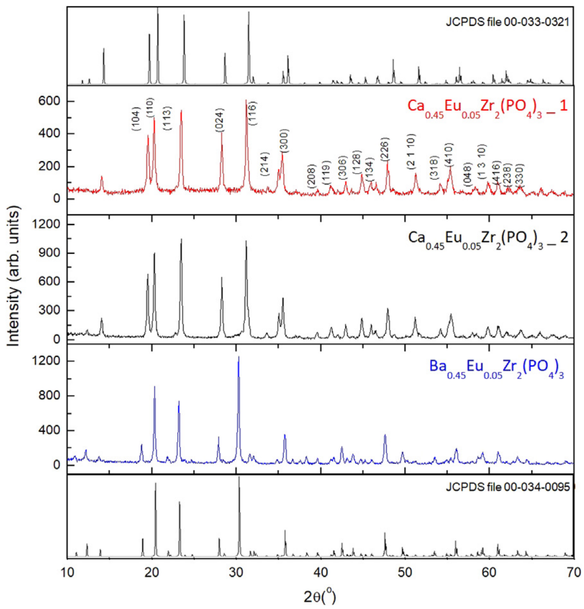

Fig. 1. XRD patterns of M0.45Eu0.05Zr2(PO4)3 samples.

assessed by photoluminescence (PL) measurements. The samples were performed using an excitation source Spectraphysics consisting in an unfocussed pulsed laser beam Spectraphysics of about 100 fs time duration at a workrepetition rate of 1 kHz and centered at 333 nm.

3. Results

3.1. X-ray diffraction

Fig. 1 shows a comparison of XRD patterns of synthesized $M_{0.45}Eu_{0.05}Zr_2(PO_4)_3$ samples with M = Ca or Ba. In all cases, the observed diffraction maxima can be indexed according to a rhombohedral symmetry of space group R-3 with $Z = 6$ [JCPDS file 00-033-0321and 00-034-0095], compatible with a NASICON-type structure. No secondary peaks have been observed within the sensitivity of the experimental system used, which indicates the purity of the obtained samples. In addition, higher diffraction maxima signal were found in the XRD pattern of the $Ca_{0.45}Eu_{0.05}Zr_2(PO_4)_3$_2 and $Ba_{0.45}Eu_{0.05}Zr_2(PO_4)_3$ samples. This result could be indicating that the treatment in N_2/H_2 reducing atmosphere favors the crystallinity of the samples.

Lattice parameters and cell volumes of all the synthesized samples calculated with Chekcell software [36] are shown in Table 1. The obtained lattice parameters values are in agreement with those previously reported [7] for powders prepared by sol-gel and subsequent treatment in reducing atmosphere. Slightly higher lattice parameters were obtained for the $Ba_{0.45}Eu_{0.05}Zr_2(PO_4)_3$ sample. For the $Ca_{0.45}Eu_{0.05}Zr_2(PO_4)_3$ samples, the parameters obtained were very similar, although slightly longer to the sample treated under N_2/H_2 atmosphere. The differences obtained for $Ca_{0.45}Eu_{0.05}Zr_2(PO_4)_3$_2 and $Ba_{0.45}Eu_{0.05}Zr_2(PO_4)_3$ samples are in good agreement with the corresponding Shannon radii [37] of M^{2+} cations, all in the environment of six coordination of the NASICON-type structure (r (Ca^{2+})) = 1.00 Å; r

Table 1
Crystallographic parameters and average particle size of $M_{0.45}Eu_{0.05}Zr_2(PO_4)_3$samples.

Samples	a = b (Å)	c (Å)	V (Å³)	D_m (nm)
$Ca_{0.45}Eu_{0.05}Zr_2(PO_4)_3$_1	8.775(3)	22.714(6)	1748,99(2)	58
$Ca_{0.45}Eu_{0.05}Zr_2(PO_4)_3$_2	8.796(2)	22.768(4)	1761,55(2)	72
$Ba_{0.45}Eu_{0.05}Zr_2(PO_4)_3$	8.652(8)	23.926(9)	1791,03(1)	85

(Ba^{2+}) = 1.36 Å (r (Eu^{2+}) = 1.17 Å).

The average crystallite size was estimated from the most intense reflections observed in the XRD patterns: (1 0 4), (1 1 0), (1 1 3) and (1 1 6) by the Scherrer equation [38]. As can be seen in Table 1, the average crystallite sizes range between 58 and 85 nm. A larger crystallite size is found in $Ba_{0.45}Eu_{0.05}Zr_2(PO_4)_3$, $Ca_{0.45}Eu_{0.05}Zr_2(PO_4)_3$_2 samples. This result confirms that the treatment in a N_2/H_2 reducing atmosphere favors the crystallinity of the samples, since a smaller crystal size is found in the calcium sample treated in an N_2 atmosphere. Particles on the nano scale are obtained in all cases. In addition, calcium by barium substitution leads to a powder formed by larger particles.

X-ray diffraction data were refined by the Rietveld method according to a NASICON type structure, where calcium and barium atoms were distributed in the 3a (0, 0, 0) and 3b (0, 0, 0.5) special sites, zirconium were located at 6c (0, 0, z) positions and phosphorus and oxygen at 18 f (x, y, z) sites. All refinements were carried considering that the calcium or barium and europium atoms were randomly located in the 3a and 3b sites with an occupation rate of 90% and 10%, respectively, in agreement with structural studies carried out by Hirayama et al. [18]. The atomic positions, refined R-factors M-O and bond distances are shown in Tables 2, 3. The R-factors and the observed, calculated and difference XRD patterns obtained in these refinements (Fig. 2) are good agreement with the model proposed.

Refined M-O bond distances are in good agreement with those obtained from the sum of the corresponding Shannon ionic radii [37]. Regarding the (Ca/Ba)/Eu (3a site)-O and (Ca/Ba)/Eu (3b site)-O bond distances, larger (Ca/Ba)/Eu (3b site)-O distance is always found as compared with the corresponding ((Ca/Ba)/Eu (3a site)-O) distance, especially in the calcium samples. These results are similar to those published in a previous work [7]. In addition, larger (3a site)-O and (3b site)-O bond lengths are also found for the $Ba_{0.45}Eu_{0.05}Zr_2(PO_4)_3$ sample compared with the calcium samples, in good agreement with Shannon's ionic radii [37]. It is noted that these bond distances are measured along the c-axis of the structure and, therefore, larger bond distances lead to greater c parameter, so these results are in agreement with the cell parameters calculated from the corresponding XRD patterns (see Table 2).

A perspective of $M_{0.45}Eu_{0.05}Zr_2(PO_4)_3$ structure along the ac plane is shown in Fig. 3. [ZrO_6] octahedral sharing corners with six isolated [PO_4] tetrahedral can be observed while in the interstitial sites calcium or barium and europium atoms are randomly distributed in the M1 and M2 positions.

3.2. Fourier transform infrared spectroscopy

Comparative FTIR spectra of $M_{0.45}Eu_{0.05}Zr_2(PO_4)_3$ and $M_{0.45}Eu_{0.05}Zr_2(PO_4)_3$ @SiO_2 samples are shown in Fig. 4. The obtained spectra are similar in terms of the band positions. Several absorption bands can be appreciated in the 4000–400 cm^{-1} range. The observed band peaked at 3500 cm^{-1} can be attributed to the OH bending vibration [39] of water adsorbed in the KBr used in the elaboration of the pellets. In FTIR spectra of $M_{0.45}Eu_{0.05}Zr_2(PO_4)_3$ the absorption bands in the range 1185–1020 cm^{-1} and 989–982 cm^{-1} was ascribed to υ_3 asymmetrical and $\upsilon_1$symmetrical stretching vibrations of PO_4^{3-} unit, respectively. The bands centered between 643 and 552 cm^{-1} are attributed to δ(O–P–O) bending [23,24]. Some differences can be seen in the FTIR spectra of $M_{0.45}Eu_{0.05}Zr_2(PO_4)_3$ @SiO_2 samples. The adsorption bands between 802 and 794 cm^{-1} can be assigned to Si-O bending vibration modes [40,41]. In addition, the increase in the intensity of the absorption bands between 460 and 467 cm^{-1} can be justified by the overlap of the rocking vibration modes of the Si-O bonds which appear at 458 cm^{-1} [40,41]. These bands are not seen in the FITR spectrum of the $Ba_{0.45}Eu_{0.05}Zr_2(PO_4)_3$ @SiO_2 sample, which seems to indicate the absence of silica in the environment of the barium-europium luminescent core. On the other hand, the bands corresponding to the vibration

Table 2
Lattice parameters, atomic positions and refined Rietveld R-factors of $M_{0.45}Eu_{0.05}Zr_2(PO_4)_3$ samples.

Samples	$Ca_{0.45}Eu_{0.05}Zr_2(PO_4)_3$_1			$Ca_{0.45}Eu_{0.05}Zr_2(PO_4)_3$_2			$Ba_{0.45}Eu_{0.05}Zr_2(PO_4)_3$		
a = *b*	8.7738(7)			8.7747(7)			8.6531(8)		
c	22.7126(1)			22.7162(1)			23.9215(3)		
Atomic positions	**x**	**y**	**z**	**x**	**Y**	**z**	**x**	**y**	**z**
Ca1/Ba1	0	0	0	0	0	0	0	0	0
Ca2/Ba2	0	0	0.5	0	0	0.5	0	0	0.5
Zr1	0	0	0.148(2)	0	0	0.147(1)	0	0	0.150(8)
Zr2	0	0	0.642(5)	0	0	0.642(6)	0	0	0.648(2)
P	0.283(1)	0.990(4)	0.255(7)	0.291(7)	0.990(6)	0.255(5)	0.281(6)	0.989(9)	0.248(6)
O1	0.177(2)	0.985(5)	0.195(5)	0.202(6)	0.979(6)	0.199(2)	0.179(2)	0.979(2)	0.200(5)
O2	0.061(9)	0.812(9)	0.691(8)	0.031(5)	0.837(2)	0.697(5)	0.009(2)	0.832(3)	0.821(4)
O3	0.203(2)	0.162(5)	0.084(8)	0.212(3)	0.153(6)	0.089(2)	0.189(3)	0.195(2)	0.094(7)
O4	0.805(6)	0.807(3)	0.579(5)	0.830(6)	0.826(8)	0.586(1)	0.848(9)	0.784(5)	0.595(7)
R-factors	R_p:15.3 R_{wp}:17.5 R_F:3.41 R_B:5.35			R_p:11.5 R_{wp}:12.7 R_F:2.25 R_B:3.62			R_p:16.6 R_{wp}:30.8 R_F:4.61 R_B:4.81		

of Si-O-Si (1100 cm^{-1}) stretching modes and to the O-Si-O (1220 cm^{-1}) silica bonds [42], which would also indicate the presence of SiO_2 in the prepared samples, are not observed because these bands are coincident with those corresponding to the modes asymmetrical stretching vibrations of PO_4^{3-} unit. Silica presence is evident in the spectra of $Ca_{0.45}Eu_{0.05}Zr_2(PO_4)_3$_1@$SiO_2$ and $Ca_{0.45}Eu_{0.05}Zr_2(PO_4)_3$_2@$SiO_2$ samples (see Fig. 4), since adsorption bands assigned to the rocking vibration modes of the Si-O bonds can be clearly observed at 460 and 466 cm^{-1}. In the spectrum of the $Ba_{0.45}Eu_{0.05}Zr_2(PO_4)_3$@$SiO_2$ sample does not observed. This phenomenon is again evident in the spectrum of the $Ba_{0.45}Eu_{0.05}Zr_2(PO_4)_3$@$SiO_2$_9 sample, obtained by increasing the reaction time of the luminescent core with TEOS (see adsorption band at 460 cm^{-1}).

3.3. Transmission electron microscopy

Figs. 5, 6 and 7 show TEM images of $M_{0.45}Eu_{0.05}Zr_2(PO_4)_3$ and $M_{0.45}Eu_{0.05}Zr_2(PO_4)_3$ @SiO_2 samples. Nanoparticles agglomerated with an average particle size of 55 nm which are covered by an amorphous layer of silica of 19 nm thickness is observed in Fig. 5b. Moreover, nanoparticles of 71 nm average particle size covered by an amorphous layer of 20 nm can be appreciate in Fig. 6b. In both cases, nanoparticles are shown whose size is in good agreement with the values determined by the Scherrer equation [38] from the XRD patterns (Fig. 1). On the other hand, particles agglomerated with an average particle size of 74 nm can be appreciated in $Ba_{0.45}Eu_{0.05}Zr_2(PO_4)_3$ sample (Fig. 7a), again in concordance with the size calculated from Sherrer formula [38]. TEM image of $Ba_{0.45}Eu_{0.05}Zr_2(PO_4)_3$@$SiO_2$ sample (Fig. 7b) shows again nanoparticles agglomerates and the silica shell presence is not detected. This evidence is in good agreement with the FTIR of this sample (see Fig. 4). The increase of the reaction time of $Ba_{0.45}Eu_{0.05}Zr_2(PO_4)_3$ core with TEOS generates the $Ba_{0.45}Eu_{0.05}Zr_2(PO_4)_3$@$SiO_2$_9 sample (Fig. 7c), which does show aggregates nanoparticles surrounded by a homogeneous silica layer of 36 nm of thickness. The increase of the reaction time extends the thickness of the shell. These results have been previously reported in covered nanophosphors, but with other stoichiometry [30].

As an example, EDS microanalysis carried out in different areas of the images for the $M_{0.45}Eu_{0.05}Zr_2(PO_4)_3$ and $M_{0.45}Eu_{0.05}Zr_2(PO_4)_3$@$SiO_2$ samples are exhibit in Fig. 8.

Obtained spectra are exhibit in Fig. 8. In the analysis corresponding to the cores, the expected compositions for the samples were observed. Moreover, the silica presence can be clearly appreciated in the covered samples analysis.

3.4. Magnetic susceptibility measurements

Fig. 9 shows the variation of the inverse magnetic susceptibility with temperature for all $M_{0.45}Eu_{0.05}Zr_2(PO_4)_3$ synthetized samples with M = Ca or Ba. A linear behavior is appreciable in the temperature range between 80 and 300 K for the $Ca_{0.45}Eu_{0.05}Zr_2(PO_4)_3$_2 and $Ba_{0.45}Eu_{0.05}Zr_2(PO_4)_3$ samples (see Fig. 9a). The calculated effective magnetic moment is 6.9 μB and 6.03 μB, respectively. In the first case, this moment is practically equivalent to the Eu^{2+} ion isolated in the $4f^7$ configuration (7 μB) [7] and significantly different to the Eu^{3+} ion (3.4 μB) [43]. These results confirm the presence of Eu^{2+} ion in the calcium sample and a certain proportion of Eu^{3+} ions in the barium sample. These results show that the N_2:H_2 reducing atmosphere has allowed the total reduction of the oxidation state of europium from 3 + to 2 + in the calcium sample but not in the barium sample. Considering the relations: $\mu^2_{exp} = x_1\mu^2_{Eu^{3+}} + x_2\mu^2_{Eu^{2+}}$ and $x = x_1 + x_2$ [46], the percentage of Eu^{3+} and Eu^{2+} ions has been calculated. The calculations made show an Eu^{2+}/Eu^{3+} ratio of 0.66/0.34 in the $Ba_{0.45}Eu_{0.05}Zr_2(PO_4)_3$ sample, which indicates that the use of a N_2/H_2 reducing atmosphere in these synthesis has reached a reduction around of 70%, far from the 97% obtained in the case of

Table 3
Bond distances obtained from refined Rietveld of $M_{0.45}Eu_{0.05}Zr_2(PO_4)_3$ samples.

	$Ca_{0.45}Eu_{0.05}Zr_2(PO_4)_3$_1	$Ca_{0.45}Eu_{0.05}Zr_2(PO_4)_3$_2	$Ba_{0.45}Eu_{0.05}Zr_2(PO_4)_3$
d (Zr1-O) Å	2.121(4) x 3	1.944(6) x 3	2.031(7) x 3
	2.217(9) x 3	2.182(3) x 3	2.174(1) x 3
d (Zr2-O) Å	1.974(6) x 3	2.121(6) x 3	2.080(3) x 3
	2.017(8) x 3	2.243(6) x 3	2.233(9) x 3
d (P-O) Å	1.476(9)	1.434(5)	1.428(6)
	1.550(2)	1.589(8)	1.474(5)
	1.518(4)	1.448(3)	1.537(5)
	1.577(8)	1.404(9)	1.548(7)
d [(Ca/Ba)/Eu (3a-O)] Å	2.466(4) x 6	2.481(1) x 6	2.812(6) x 6
d [(Ca/Ba)/Eu (3b-O)] Å	2.624(2) x 6	2.529(2) x 6	2.826(6) x 6
Theoretical bond distances (Å)	d (P^{5+}-O) = 1.550; d (Zr^{4+}-O) = 2.120; d (Ca^{2+}-O) = 2.400; d (Ba^{2+}-O) = 2.760; d (Eu^{2+}-O) = 2.570; d (Eu^{3+}-O) = 2.347		

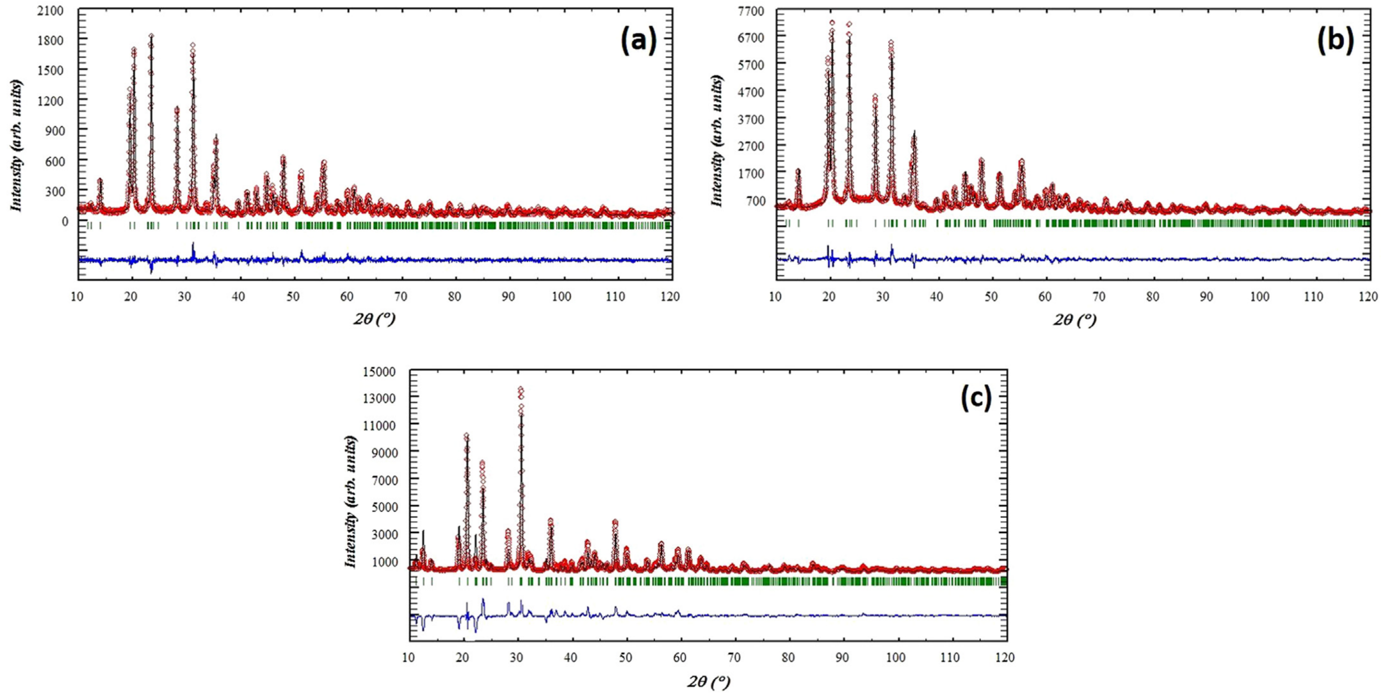

Fig. 2. XRD patterns of: (a) $Ca_{0.45}Eu_{0.05}Zr_2(PO_4)_3$_1, (b) $Ca_{0.45}Eu_{0.05}Zr_2(PO_4)_3$_2 and (c) $Ba_{0.45}Eu_{0.05}Zr_2(PO_4)_3$ samples.

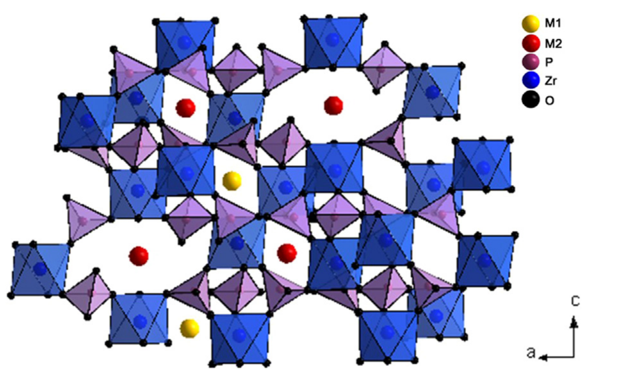

Fig. 3. Schematic perspective of the structure of $M_{0.45}Eu_{0.05}Zr_2(PO_4)_3$ samples.

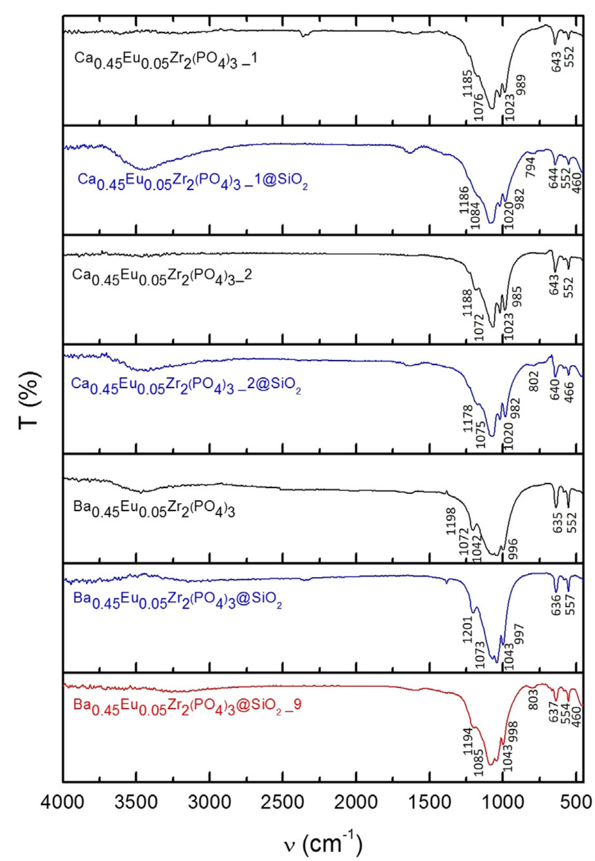

Fig. 4. Infrared spectra of $M_{0.45}Eu_{0.05}Zr_2(PO_4)_3$ and $M_{0.45}Eu_{0.05}Zr_2(PO_4)_3$@ SiO_2 samples.

$Ca_{0.45}Eu_{0.05}Zr_2(PO_4)_3$_2 sample. For $Ca_{0.45}Eu_{0.05}Zr_2(PO_4)_3$_1 sample, it is clearly observed (Fig. 9) the presence of a more complex behavior, directly related with the presence of a great amount of related to the non-reduction of Eu^{3+} ions. At higher temperatures, a characteristic Curie–Weiss paramagnet behavior can be observed while between 75 and 25 K a rise in magnetic susceptibility that tends to decreases it becomes clear. The first observed trend is in accordance with the presence in the sample of Eu^{2+} ions [7], while the second, which is in good agreement with the results described by Aitasalo et al. [44] also denotes the existence of a large percentage of Eu^{3+} ions.

3.5. Photoluminescence study

Fig. 10 shows PL spectra of of $M_{0.45}Eu_{0.05}Zr_2(PO_4)_3$ and $M_{0.45}Eu_{0.05}Zr_2(PO_4)_3$ @SiO_2 samples. Calculated color coordinates are also included in the corresponding figures. As can be observed, the spectral distribution of the emission is very similar in the $Ca_{0.45}Eu_{0.05}Zr_2(PO_4)_3$_2 and $Ba_{0.45}Eu_{0.05}Zr_2(PO_4)_3$ samples and their corresponding nanocomposites. A broad and asymmetric band is observed peaked at about 490 and 440 nm, respectively. The displacement broadband towards shorter wavelengths can be justified by consideration of Shannon ion radii of the divalent cations in a six coordination environment of oxygen [r (Ca^{2+}) = 1.00 Å and r (Ba^{2+}) = 1.35 Å] [37], which originates in a longer (Ba/Eu)-O bond distance in relation to (Ca/Eu)-O. A minor splitting of energy levels by effect of crystalline field occurs with the increase of Eu-O bond distance [18]. In the PL

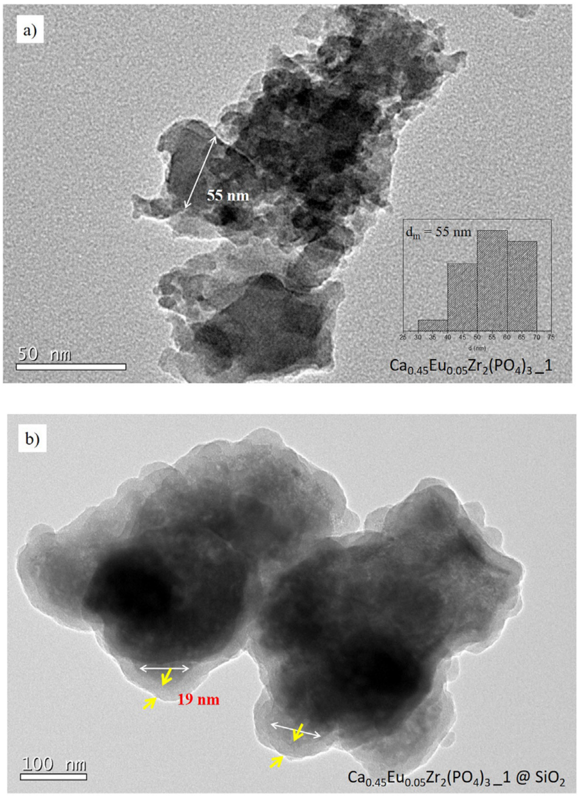

Fig. 5. TEM images of $Ca_{0.45}Eu_{0.05}Zr_2(PO_4)_3$_1 samples.

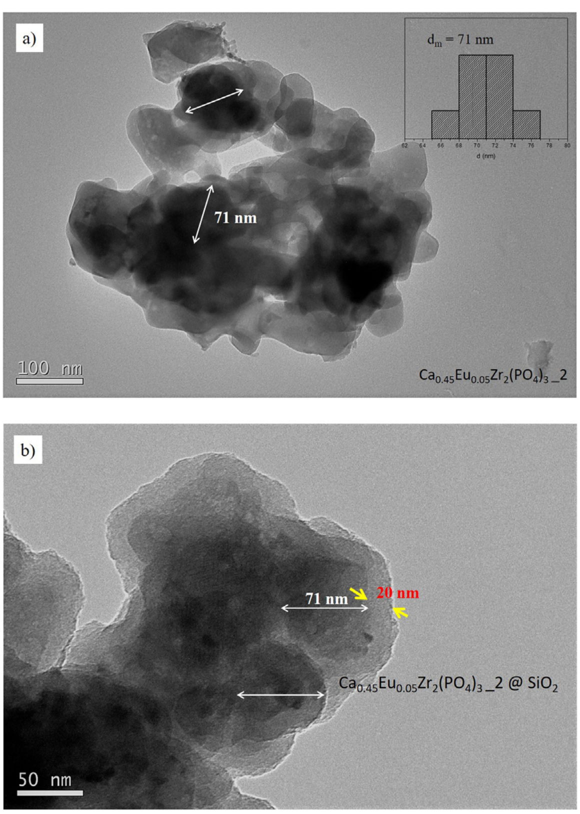

Fig. 6. TEM images of $Ca_{0.45}Eu_{0.05}Zr_2(PO_4)_3$_2 samples.

spectra of $Ca_{0.45}Eu_{0.05}Zr_2(PO_4)_3$_2 sample (Fig. 10a), sharp PL emission lines corresponding to Eu^{3+} 4–4f intraionic transitions were not found, supporting a complete reduction of the europium ions in good

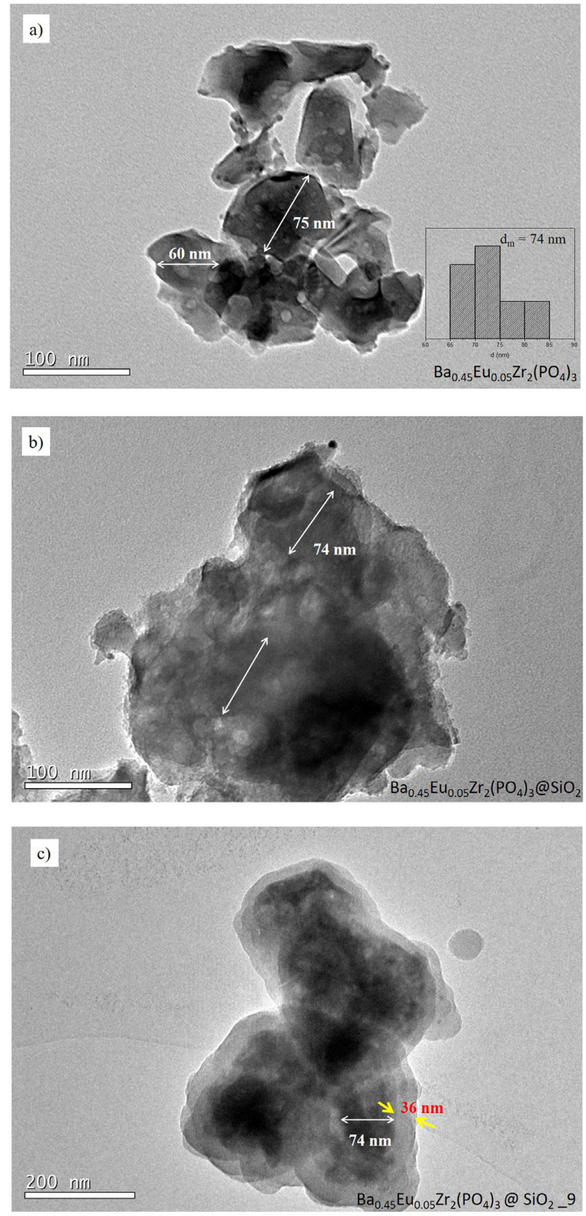

Fig. 7. TEM images of $Ba_{0.45}Eu_{0.05}Zr_2(PO_4)_3$ samples.

agreement with magnetic study discussed above. Unlike, for the $Ba_{0.45}Eu_{0.05}Zr_2(PO_4)_3$ samples it is possible to notice the existence subtle of narrower peaks at 593 and 613 nm (see Fig. 10b) which can be assigned to the $^5D_1$–$^7F_3$ and $^5D_0$–$^7F_2$, transitions of Eu^{3+} ions. This result evidences a non-complete reduction o of $Eu^{3\ +}$ to Eu^{2+} ions in this sample, which appear much more marked in the PL spectra of the sample t $Ca_{0.45}Eu_{0.05}Zr_2(PO_4)_3$_1 (see Fig. 10c), where can be observed narrower peaks between 570 and 700 nm assigned to the $^5D_0$–^7F_J (J = 1–4) transitions of Eu^{3+}, being $^5D_0$–$^7F_2$ dominant. This result has also been confirmed from the magnetic measurements.

Previous PL investigations reveal that the Eu^{2+} emission consists of two bands attributed to the existence of two different luminescence centers, which can be associated to the M1 and M2 positions of the NASICON-type structure present in the investigated samples [7]. The obtained results indicate, according to the refinement of XRD data, that Eu^{2+} or Eu^{2+} ions occupy two different positions in the lattice or two equivalent positions but with different oxygen coordination in the synthesized samples.

By consideration of the PL spectra of $M_{0.45}Eu_{0.05}Zr_2(PO_4)_3@SiO_2$

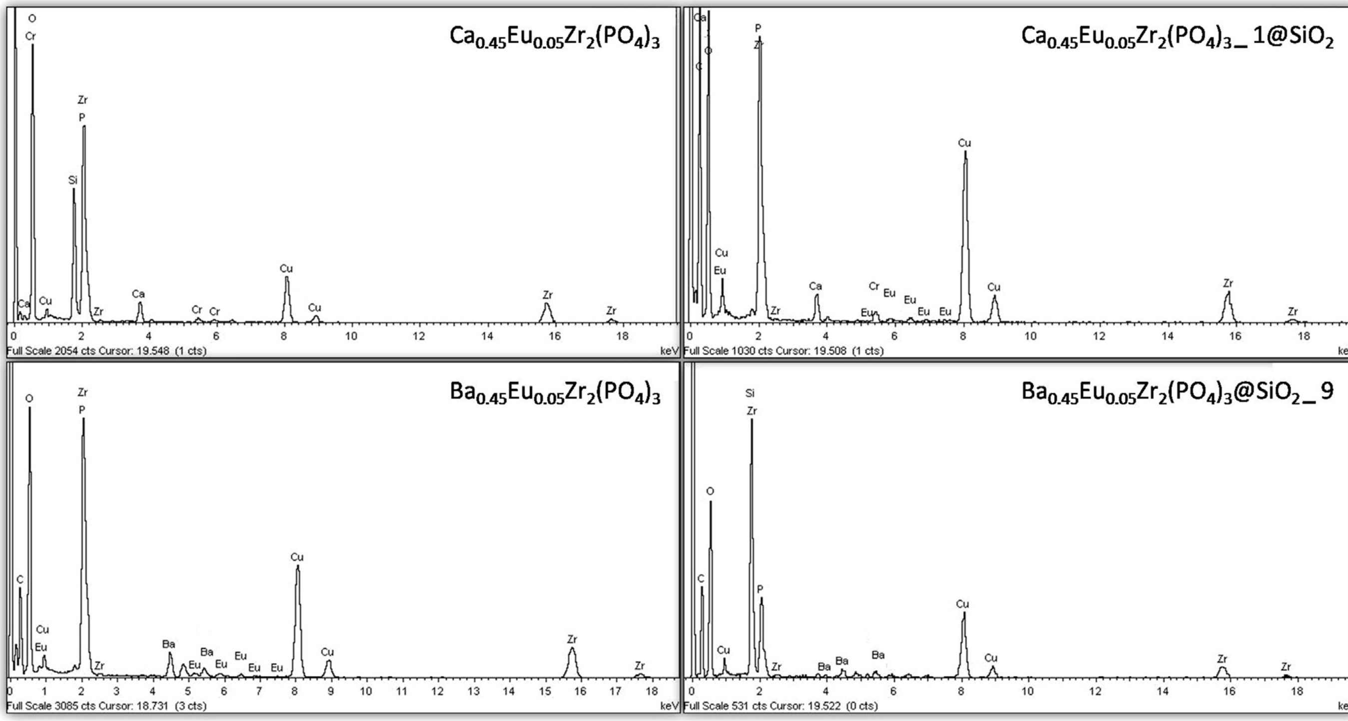

Fig. 8. EDS microanalysis of the $M_{0.45}Eu_{0.05}Zr_2(PO_4)_3$ and $M_{0.45}Eu_{0.05}Zr_2(PO_4)_3@SiO_2$ samples.

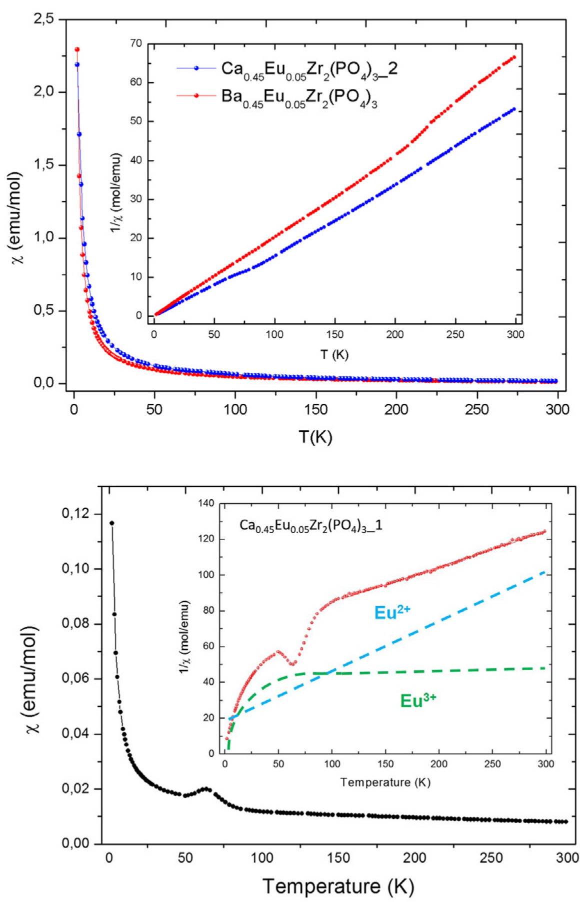

Fig. 9. Variation of magnetic susceptibility vs. temperature of $M_{0.45}Eu_{0.05}Zr_2(PO_4)_3$ samples.

samples (Fig. 10), can be observed that the amorphous silica covering (of the order of 20 nm as identified in TEM images) improved the emission intensity in a high percentage. This effect is much more marked in the PL spectra of $Ba_{0.45}Eu_{0.05}Zr_2(PO_4)_3$ @SiO_2 in relation to $Ca_{0.45}Eu_{0.05}Zr_2(PO_4)_3$_2@$SiO_2$, indicating that this sample is a better phosphor emitter. These results can be explained taking into account that the surface defects present in the nanoparticles of the synthesized samples provide non-radiative recombination channels for electrons and holes, which leads to a reduced photoluminescence quantum yield. The covering with a homogeneous silica shell decreases these defects.

In the PL spectrum of $Ca_{0.45}Eu_{0.05}Zr_2(PO_4)_3$_1@$SiO_2$_9h sample (Fig. 10c), a notable reduction of luminescent emission can be observed, so it is possible to think that the increase of the thickness of the silica shell (36 nm) and the presence of silanol groups in the silica can act as luminescence quenchers [30,45].

Fig. 10 also shows the obtained calculated CIE chromaticity coordinates of the samples prepared. The samples $Ca_{0.45}Eu_{0.05}Zr_2(PO_4)_3$_2 and $Ca_{0.45}Eu_{0.05}Zr_2(PO_4)_3$_2@$SiO_2$ show blue-green emission located at (0.243, 0.380), irrespectively of the covered or uncovered sample. However, in the samples $Ca_{0.45}Eu_{0.05}Zr_2(PO_4)_3$_1 and $Ca_{0.45}Eu_{0.05}Zr_2(PO_4)_3$_1@$SiO_2$ the calculated CIE chromaticity coordinates are located at (0.288, 0.250) and (0.281, 0.229), respectively, showing how the shell slightly shifts the emission towards the blue. This same phenomenon is observed in the $Ba_{0.45}Eu_{0.05}Zr_2(PO_4)_3$@$SiO_2$ and $Ba_{0.45}Eu_{0.05}Zr_2(PO_4)_3$@$SiO_2$ _9h samples where CIE coordinates are located at (0.205, 0.130) and (0.196, 0.117). However, regardless of these nearby emission, it is possible to concluded that all the investigated nanophosphors can be efficiently excited by near-UV light, indicating that the phosphors are promising green or blue phosphors candidate for LEDs. The results suggest that the prepared phosphors exhibit great potential for use as single-phase full-color phosphor, in combination with yellow light phosphors, for near ultraviolet white light emitting diodes (NUV WLEDs).

4. Conclusions

$M_{0.45}Eu_{0.05}Zr_2(PO_4)_3$ nanophosphors and their corresponding silica

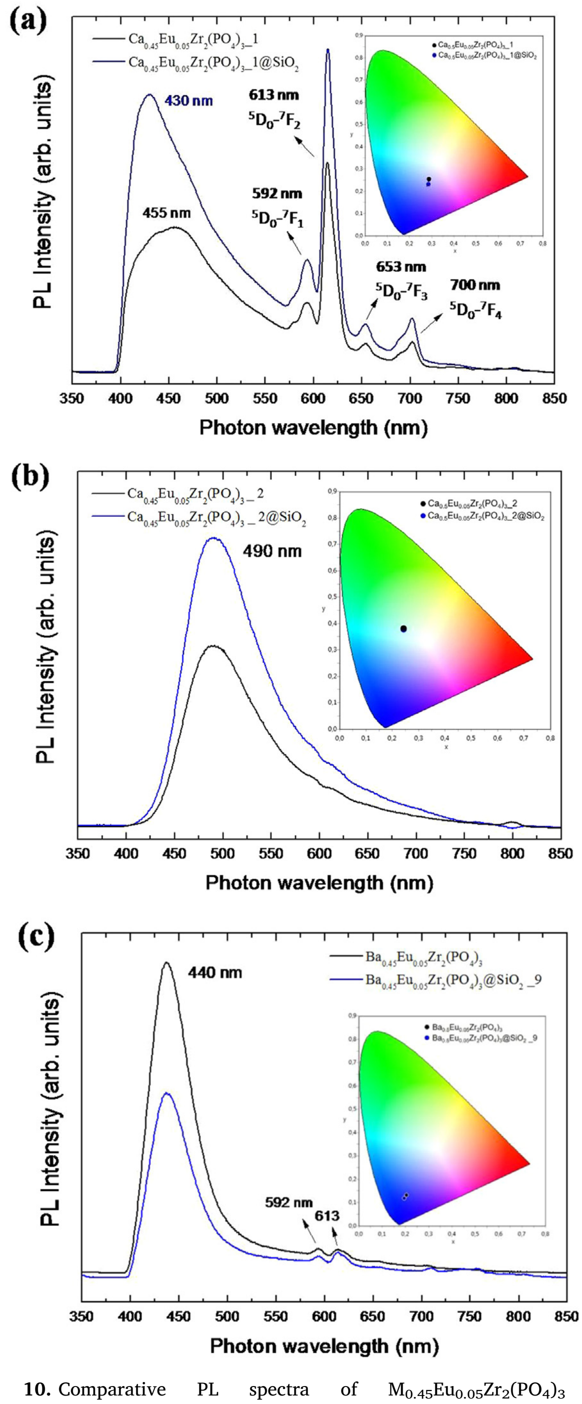

Fig. 10. Comparative PL spectra of $M_{0.45}Eu_{0.05}Zr_2(PO_4)_3$ and $M_{0.45}Eu_{0.05}Zr_2(PO_4)_3@SiO_2$ samples. In addition, the CIE chromaticity diagrams are included.

nanocomposites were obtained. The investigated luminescent cores were synthesized by a sol-gel method and subsequently treated in a N_2 or N_2/H_2 reducing atmosphere in order to stabilize the 2 + oxidation state of the europium cation. XRD patterns of the cores samples show diffraction maxima compatibles with a NASICON-type structure. Several absorption bands attributed to PO_4^{3-} unit were found in the FTIR spectra of the $M_{0.45}Eu_{0.05}Zr_2(PO_4)_3$ samples. The presence of silica has been shown in the spectra of all nanocomposites except for the one in the $Ba_{0.45}Eu_{0.05}Zr_2(PO_4)_3@SiO_2$ sample. TEM images of the $M_{0.45}Eu_{0.05}Zr_2(PO_4)_3@SiO_2$ samples reveals nanoparticles of average size crystallite of 55, 71 y 74 nm for $Ca_{0.45}Eu_{0.05}Zr_2(PO_4)_3$_2, $Ca_{0.45}Eu_{0.05}Zr_2(PO_4)_3$_1 and $Ba_{0.45}Eu_{0.05}Zr_2(PO_4)_3$ samples, respectively and a homogeneous silica covering in the nanocomposites. This shell is not evident in the $Ba_{0.45}Eu_{0.05}Zr_2(PO_4)_3@SiO_2$ sample The thickness of the silica shell is the same in samples treated during 3 h with TEOS and increases when the reaction with TEOS takes place over 9 h. Magnetic measurements reveals that that only for the $Ca_{0.45}Eu_{0.05}Zr_2(PO_4)_3$ sample treated in a N_2/H_2 reducing atmosphere, a total reduction of Eu^{3+} and Eu^{2+} is achieved. In the other two luminescent cores, the coexistence of Eu^{2+} and Eu^{3+} cations is detected. Broad emission bands was observed in the PL spectra of $Ca_{0.45}Eu_{0.05}Zr_2(PO_4)_3$_2, assignable to the 4f-5d transitions of the Eu^{2+} ions. In addition, some sharp emission lines were found in the spectra corresponding to $Ca_{0.45}Eu_{0.05}Zr_2(PO_4)_3$_1 and $Ba_{0.45}Eu_{0.05}Zr_2(PO_4)_3$ samples attributed to the 4–4f intraionic transitions of Eu^{3+} ions. The covering with a homogeneous silica shell decrease the surface defects of luminescent cores, leading to an enhance of the PL intensity and increasing their utility in different luminescent devices because exhibit great potential for use as single-phase full-color phosphor, in combination with yellow light phosphors, for near ultraviolet white light emitting diodes (NUV WLEDs).

Acknowledgments

Fundación Neurociencias y Envejecimiento has supported this work through project 359/2014 as well as MINECO through the project MAT2016-80182-R. The authors thank the ICTS National Center for Electron Microscopy of the UCM for access.

References

[1] D. Dosev, M. Nichkova, R.K. Dumas, S.J. Gee, B.D. Hammock, K. Liu, I.M. Kennedy, Magnetic/luminescent core/shell particles synthesized by spray pyrolysis and their application in immunoassays with internal standard, Nanotechnology 18 (2007) 055102.

[2] G. Blasse, B.C. Grabmaier, Luminescent Materials, Springer, Berlin, 1994.

[3] C.R. Ronda, Phosphors for lamp and displays: an application view, J. Alloy Compd. 225 (1995) 534–538.

[4] C.R. Ronda, Recent achievements in research on phosphors for lamps and displays, J. Lumin. 72–74 (1997) 49–54.

[5] K.N. Shinde, S.J. Dhoble, H.C. Swart, K. Park, Phosphate Phosphors for Solid-state Lighting, Springer, Berlín, Germany, 2012.

[6] L. Alcaraz, J. Isasi, M. Peiteado, A. Caballero, Síntesis, caracterización estructural y morfológica de nanofósforos $Ca_{0.45}Eu_{0.05}Zr_2(PO_4)_3$, Bol. De. la Soc. Esp. De. Cerámica Y. Vidr. 54 (2015) 236–240.

[7] L. Alcaraz, J. Isasi, C. Díaz-Guerra, M. Peiteado, A. Caballero, Preparation of $Ca_{0.5}Zr_2(PO_4)_3$ and $Ca_{0.45}Eu_{0.05}Zr_2(PO_4)_3$ nanopowders: structural characterization and luminescence emission stud, J. Phys. D Appl. Phys. 49 (2016) 115501.

[8] Y. Qiao, X. Zhang, X. Ye, Y. Chen, H. Guo, Photoluminescent properties of $Sr_2SiO_4:Eu^{3+}$ and $Sr_2SiO_4:Eu^{2+}$ phosphors prepared by solid-state reaction method, J. Rare Earths 27 (2009) 323–327.

[9] I. Omkaran, B.V. Rao, S. Buddhudu, Photoluminescence properties of Eu^{3+}:$mgal_2O_4$ powder phosphor, J. Alloy Compd. 474 (2009) 565–568.

[10] R.S. Yadav, R.K. Dutta, M. Kumar, A.C. Pandey, Improved color purity in nano-size Eu^{3+}-doped YBO_3 red phosphor, J. Lumin. 129 (2009) 1078–1082.

[11] M.M. Haque, H.L. Lee, D.K. Kim, Luminescent properties of Eu^{3+}-activated molybdate-based novel red-emitting phosphors for LEDs, J. Alloy. Compd. 481 (2009) 792–796.

[12] S. Shionoya, W.M. Yen, Phosphor Handbook (Phosphor Research society), CRC Press, Boca Raton, 1998.

[13] J. Yu, C. Guo, Z. Ren, J. Bai, Photoluminescence of double-color-emitting phosphor $Ca_5(PO_4)_3Cl:Eu^{2+}$, Mn^{2+} for near-UV LED, Opt. Laser Technol. 43 (2011) 762–766.

[14] E. Siebert, P. Fabry, NASICON type ionic conductors for alkali ion sensing, Ionics 5 (1999) 61–268.

[15] R. Prasada Rao, C. Maohua, S. Adams, Preparation and characterization of NASICON type Li^+ ionic conductors, J. Solid State Electr. 16 (2012) 3349–3354.

[16] A. Mbandza, E. Bordes, P. Courtine, A. El Jazouli, J.L. Soubeyroux, G. Le Flem, P. Hagenmuller, The nasicon-type copper(I) titanium phosphate $CuTi_2(PO_4)_3$: structure and chemical properties, React. Solid 5 (1988) 315–321.

[17] A. El Jazouli, A. Nadiri, J.M. Dance, C. Delmas, G. Le Flem, P. Hagenmuller, Relationships between structure and magnetic properties of titanium (III) nasicon-type phosphates, J. Phys. Chem. Solids 49 (1988) 779–783.

[18] M. Hirayama, N. Sonoyama, A. Yamada, R. Kanno, Structural investigation of Eu^{2+} emissions from alkaline earth zirconium phosphate, J. Solid State Chem. 182 (2009) 730–735.

[19] T. Masui, K. Koyabu, S. Tamura, N. Imanaka, Synthesis of a new NASICON-type blue luminescent material, J. Alloy. Compd. 418 (2006) 73–76.

[20] J. Wang, Z.-J. Zhang, Luminescence properties and energy transfer studies of color tunable Tb^{3+} -doped $RE_{1/3}Zr_2(PO_4)_3$ (RE = Y, La, Gd and Lu), J. Alloy. Compd. 685

(2016) 841–847.

[21] D.Y. Xie, Z.H. Wang, X.S. Liu, W.B. Song, B.H. Yuan, E.J. Liang, Rapid synthesis of low thermal expansion materials of $Ca_{1-x}Sr_xZr_4P_6O_{24}$, Ceram. Int. 38 (2012) 3807–3813.

[22] S. Yang, W. Que, J. Chen, et al., Nd: yag nano-crystalline powders derived by combining co-precipitation method with citric acid treatment, Ceram. Int. 38 (2012) 3185–3189.

[23] Z.-w. Zhang, L. Liu, X.-f. Zhang, J.-p. Zhang, W.-g. Zhang, D.-j. Wang, Preparation and investigation of $CaZr_4(PO_4)_6$:Dy^{3+} single-phase full-color phosphor, Spectrochim. Acta A 137 (2015) 1–6.

[24] G. Ju, Y. Hu, L. Chen, Y. Jin, S. Zhang, F. Xue, H. Chen, Self-activated photo-luminescence and persistent luminescence in$CaZr_4(PO_4)_6$, Mater. Res. Bull. 83 (2016) 211–216.

[25] R. Hepzi, P. Devamani, M. Alagar, Synthesis and characterization of aluminium phosphate nanoparticles, Int. J. Appl. Sci. Eng. Res. 1 (2012) 769–775.

[26] B. Raina, D. Singh, K.K. Bamzai, Co-precipitation synthesis, characterization, thermal and spectroscopic analysis of gadolinium-doped neodymium phosphate nanoparticles, J. Therm. Anal. Calorim. 130 (2017) 1829–1845.

[27] L. Alcaraz, J. Isasi, M. Fernández, C. Díaz-Guerra, Effect of synthesis conditions on the structural characterization and luminescence properties of $Y_{0.9}Eu_{0.1}V_{1-x}Cr_xO_4$ ($0 \le x \le 0.5$) nanopowders, Mater. Chem. Phys. 145 (2014) 18–26.

[28] L. Alcaraz, J. Isasi, A.C. Caballero, J.G. Izquierdo, L. Bañares, Nanopowders $Y_{1-y}Nd_yV_{1-x}Cr_xO_4$ with y = 0 and 1; x = 0. 0.1, 0.2, 0.5 synthetized by a sol-gel process. Relationship between morphological characteristics and optical properties, J. Lumin. 161 (2015) 110–116.

[29] L. Alcaraz, J. Isasi, C. Díaz-Guerra, Effects of preparation method and pH variation on the structural characteristics and luminescence properties of $Y_{0.9}Er_{0.1}VO_4$ and $Y_{0.9}Er_{0.1}V_{0.9}Cr_{0.1}O_4$ nanopowders, J. Lumin. 165 (2015) 105–114.

[30] L. Alcaraz, J. Isasi, C. Díaz-Guerra, Comparative study of $Y_{0.9}Er_{0.1}V_{1-x}P_xO_4$ nanophosphors with x =;0, 0.1, 0.5, 0.9 and 1 prepared by sol-gel and hydrothermal processes, J. Alloy. Compd. 687 (2016) 754–764.

[31] L. Alcaraz, J. Isasi, Synthesis and study of $Y_{0.9}Ln_{0.1}VO_4$ nanophosphors and $Y_{0.9}Ln_{0.1}VO_4$@SiO_2 luminescent nanocomposites with Ln = Eu, Dy, Er, Ceram. Int. 43 (2017) 5311–5318.

[32] L. Liu, H. Xiao, X. An, Y. Zhang, R. Qin, L. Liu, D. Zhang, R. Sun, L. Chen, Synthesis and photoluminescence properties of core-shell structured YVO_4:Eu^{3+}@SiO_2 nanocomposites, Chem. Phys. Lett. 619 (2015) 169–173.

[33] M. Ocaña, E. Cantelar, F. Cussó, Facile single-step procedure for the synthesis of luminescent Ln^{3+}:yvo_4 (Ln = Eu or Er + Yb)-silica nanocomposites, Mater. Chem. Phys. 125 (2011) 224–230.

[34] L. Tang, K. Ding, N. Chen, G. Du, An ion adsorption-diffusion process for preparing YVO_4:Eu^{3+}@SiO_2 core-shell nanoparticles with strong luminescence, Ceram. Int. 40 (2014) 9621–9628.

[35] W. Stöber, A. Fink, E. Bohn, Controlled growth of monodisperse silica spheres in the micron sizes range", J. Colloid Interf. Sci. 26 (1968) 62–69.

[36] T. Roisnel, J. Rodriguez-Carvajal, WinPLOTR, plotr@llb.saclay.cea.fr, 〈http://www-llb.cea.fr/fullweb/winplotr/winplotr.htm〉.

[37] J. Laugier, B. Bochu, LMGP-Suite Suite of Programs for the interpretation of X-ray experiments ENSP/Laboratoire des Materiaux et du Genie Physique, France, < www.inpg. fr/LMGP > and 〈www.ccp14. ac.uk/tutorial/lmgp/〉.

[38] R.D. Shannon, Revised effective ionic radii and systematic studies of interatomic distances in halides and chalcogenides, Acta Cryst. A 32 (1976) 751–767.

[39] M.I. Mendelson, Average grain size in polycrystalline ceramics, J. Am. Ceram. Soc. 52 (1969) 443–446.

[40] D. Lin-Vien, N.B. Colthup, W.G. Fateley, J.G. Grasselli, The Handbook of IR and Raman Characteristic Frequencies of Organic Molecules, Academic Press, Cambridge, Massachusetts, USA, 1991.

[41] Y. Liang, J. Ouyang, H. Wang, W. Wang, P. Chui, K. Sun, Synthesis and characterization of core-shell structured SiO_2@YVO_4:Yb^{3+}, Er^{3+} microspheres, Appl. Surf. Sci. 258 (2012) 3689–3694.

[42] H. Wang, M. Yu, C.K. Lin, J. Lin, Core-shell structured SiO_2@YVO_4:Dy^{3+}/Sm^{3+} phosphor particles: sol-gel preparation and characterization, J. Colloid Interf. Sci. 300 (2006) 176–182.

[43] Y. Wang, W. Qin, J. Zhang, C. Cao, S. Lü, X. Ren, Photoluminescence of colloidal YVO_4:eu/sio_2 core/shell nanocrystals, Opt. Commun. 282 (2009) 1148–1153.

[44] E. Lee, Magnetism, Dover Publications, Estados Unidos, 1970.

[45] T. Aitasalo, J. Hölsä, M. Lastusaari, J. Legendziewicz, L. Lehto, J. Lindén, M. Maryško, Structural, magnetic and spectroscopic investigations of europium oxychloride, EuOCl, J. Alloy. Compd. 380 (2004) 296–302.

[46] T. Liu, W. Xu, X. Bai, H. Song, Tunable silica shell and its modification on photo-luminescent properties of Y_2O_3:Eu^{3+}@SiO_2 nanocomposites, J. Appl. Phys. 111 (2012) 064312.